




# 3D porous PTFE membrane filled with PEO-based electrolyte for all solid-state lithium–sulfur batteries

Zhen-Chao Li, Teng-Yu Li, Yi-Rui Deng, Wen-Hao Tang, Xiao-Dong Wang, Jin-Lin Yang, Qiang Liu, Lei Zhang, Qiang Wang, Rui-Ping Liu\* 

Received: 30 November 2021 / Revised: 30 December 2021 / Accepted: 17 January 2022 / Published online: 21 May 2022  
© Youke Publishing Co., Ltd. 2022

**Abstract** Owing to the low cost and high theoretical energy density, lithium–sulfur battery has become one of the most promising energy storage battery systems. However, the inherent cycle instability and safety problems of traditional liquid lithium–sulfur batteries greatly limit their commercial applications. In this work, polytetrafluoroethylene (PTFE) membrane was introduced into  $\text{Li}_7\text{La}_3\text{Zr}_2\text{O}_{12}$  (LLZO)@poly(ethylene oxide) (PEO)-based composite electrolyte as a supporting framework to prepare a new PTFE@LLZO@PEO composite electrolyte for lithium–sulfur battery. The introduction of PTFE membrane further improved the mechanical properties and thermal stability of the electrolyte. The ionic conductivity of the prepared PTFE@LLZO@PEO solid electrolyte was  $5.03 \times 10^{-5} \text{ S}\cdot\text{cm}^{-1}$  at 30 °C and  $2.54 \times 10^{-4} \text{ S}\cdot\text{cm}^{-1}$  at 60 °C. Moreover, the symmetric battery exhibited high

cycle stability (300 h). The Li–S battery based on PTFE@LLZO@PEO electrolyte exhibited excellent electrochemical performance.

**Keywords** Lithium–sulfur battery; All solid-state battery; Composite electrolyte; Shuttle effect; Lithium dendrite

## 1 Introduction

The irreversible consumption of traditional fossil energy and its environmental problems have become increasingly prominent. As a clean and efficient energy storage equipment, lithium-ion batteries are widely used in portable electronic products, electric vehicles, energy storage, and other fields [1–6]. However, the existing commercial lithium-ion batteries are getting closer to the limit of their theoretical energy density, which is insufficient for the future demand for high energy density batteries for electric vehicles and energy storage devices, especially considering the requirements for future long-haul electric vehicles [7–10]. Lithium–sulfur battery with high theoretical energy density of 2600  $\text{Wh}\cdot\text{kg}^{-1}$  and theoretical specific energy density of 1675  $\text{mAh}\cdot\text{g}^{-1}$  is considered as one of the most promising potential candidates for the next-generation energy storage system with high energy density [11–14]. Furthermore, as the cathode active material, sulfur is inexpensive, naturally abundant, and environment-friendly [15, 16]. However, the practical application of lithium–sulfur batteries is largely limited by the shuttle effect of lithium polysulfide, the internal short circuit caused by lithium dendrite growth, and the flammability of liquid electrolyte [17–24].

Many strategies have been adapted to overcome the above issues of lithium–sulfur batteries, including new cathode materials (carbon–sulfur [25], polymer-coated

Zhen-Chao Li and Teng-Yu Li have contributed equally to this work.

Z.-C. Li, T.-Y. Li, Y.-R. Deng, W.-H. Tang, X.-D. Wang, Q. Liu, R.-P. Liu\*  
Department of Materials Science and Engineering, China University of Mining & Technology (Beijing), Beijing 100083, China  
e-mail: lrp@cumtb.edu.cn

J.-L. Yang  
School of Materials Science and Engineering, Tsinghua University, Beijing 100083, China

L. Zhang  
Department of Mechanical Engineering, University of Alaska Fairbanks, PO Box 755905, Fairbanks, AK 99775, USA

Q. Wang  
Chongqing Key Laboratory of Green Aviation Energy and Power, Chongqing Jiaotong University, Chongqing 401135, China



sulfur composites [26, 27]), functional separator and interlayer [28], unique polymer adhesive [29, 30], electrolyte additive [31], and solid-state electrolytes (SSEs) [11, 18, 32, 33]. Among them, all-solid-state electrolytes (ASSEs) have been widely recognized because of their excellent potential to prevent shuttle effect and inhibit dendrite growth and high flame retardancy. Although inorganic solid electrolytes, including sulfide and oxide solid electrolytes, have high ionic conductivity and lithium-ion transfer number at room temperature, inorganic solid electrolytes also have high grain boundary resistance and poor interfacial compatibility between electrolytes and electrodes due to their high hardness and brittleness [34–36]. In contrast, polymer solid electrolyte has the advantages of easy film formation, flexibility, and good compatibility with electrode interface, which makes it easier to realize commercial application. Nevertheless, the poor ionic conductivity of polymer solid electrolyte at room temperature hinders its practical application in solid battery [37, 38]. Organic–inorganic composite solid electrolyte (CSE) combines the high ionic conductivity and mechanical strength of inorganic solid electrolyte, as well as the excellent interfacial compatibility and machinability of polymer solid electrolyte, and it is considered to be one of the most promising solid electrolyte materials for commercial applications [5, 39–41].

Solid electrolyte based on poly(ethylene oxide) (PEO) has been extensively used in the research of lithium–sulfur batteries because of its special superiority, such as strong coordination capabilities of  $\text{Li}^+$ , low cost in design, and excellent machinability [12, 42, 43]. Recently, inorganic ceramic fillers (e.g.,  $\text{Al}_2\text{O}_3$ ,  $\text{TiO}_2$ , etc.) and inorganic  $\text{Li}^+$  conductor (e.g.,  $\text{Li}_7\text{La}_3\text{Zr}_2\text{O}_{12}$ ,  $\text{Li}_{1.3}\text{Al}_{0.3}\text{Ti}_{1.7}(\text{PO}_4)_3$ ,  $\text{Li}_{0.33}\text{La}_{0.557}\text{TiO}_3$ , etc.) were added to PEO-based polymer electrolyte to improve the overall performance of PEO-based electrolytes in solid batteries [44–50]. Unfortunately, although the introduction of inorganic particles is beneficial to improve the ionic conductivity and mechanical properties of PEO-based solid electrolytes at low temperatures, the relatively low mechanical strength at high temperatures and the dissolution of polysulfides in PEO-based solid electrolytes still limit the application of PEO-based solid electrolytes in Li–S batteries [48, 51]. Polytetrafluoroethylene (PTFE) is a material with good thermal stability, non-flammability, excellent chemical stability and electrochemical stability, and good mechanical properties. In addition, PTFE is also widely used in lithium-ion batteries as an effective binder [52, 53]. Nevertheless, the application of PTFE in all-solid-state lithium–sulfur batteries is unexplored.

Herein, a PTFE@ $\text{Li}_7\text{La}_3\text{Zr}_2\text{O}_{12}$  (LLZO)@PEO composite solid electrolyte was prepared by using PEO as the polymer matrix, nano  $\text{Li}_7\text{La}_3\text{Zr}_2\text{O}_{12}$  as the inorganic filler,

and three-dimensional (3D) porous PTFE skeleton as the support structure. The introduction of PTFE not only brings strong mechanical strength, but also improves the ionic conductivity and thermal stability of PTFE@LLZO@PEO composite solid electrolyte. Meanwhile, PTFE skeleton and LLZO filler can hinder the crystallization of PEO and further improve the ionic conductivity of the electrolyte membrane. The experimental results show that PTFE@LLZO@PEO composite solid electrolyte has high ionic conductivity ( $5.03 \times 10^{-5} \text{ S}\cdot\text{cm}^{-1}$  at 30 °C), and excellent ability to inhibit the shuttle effect of lithium polysulfide and lithium dendrite growth. In addition, the assembled all-solid-state lithium–sulfur battery showed good cycle stability and rate performance. The successful preparation of PTFE@LLZO@PEO composite solid electrolyte may pave the way for the next-generation high-performance all-solid-state lithium–sulfur batteries.

## 2 Experimental

### 2.1 Preparation of composite solid electrolyte

LLZO powder was firstly heated to 400 °C and kept for 3 h under argon atmosphere to remove lithium carbonate on the surface of LLZO before use [54]. LLZO@PEO solid electrolyte and PTFE@LLZO@PEO solid electrolyte were prepared by solvent evaporation method. Firstly, 0.9 g of PEO (molecular weight ( $M_w$ ) = 300,000), 0.58722 g of bis(trifluoromethane)sulfonimide lithium salt (LiTFSI, Li:EO = 1:10), and 0.3 g of LLZO particles with the particle size of about 2  $\mu\text{m}$  were stirred and mixed in anhydrous acetonitrile solution at 60 °C for 6 h until PEO was completely dissolved to obtain LLZO@PEO slurry. Then, the uniformly mixed solution was vacuumed in the vacuum chamber for 15 min to remove the bubbles in the solution. After that, the solution was poured into a PTFE mold and dried naturally at room temperature for 24 h to form a film. After removing the solid electrolyte membrane from the mold with tweezers, the LLZO@PEO solid electrolyte was finally obtained. To obtain PTFE@LLZO@PEO solid electrolyte, the PTFE porous membrane was immersed in LLZO@PEO solution and stirred for 1 h to ensure that the pores were fully filled with the liquid. Subsequently, the porous PTFE membrane was naturally dried at room temperature for 24 h. Finally, the dried membrane was rolled twice to increase the density.

### 2.2 Preparation of sulfur cathode

The cathode was prepared by melting diffusion method. Firstly, nano-sulfur (S) and carbon nanotubes (CNTs) with weight ratio of 4:1 were ground and heated at 155 °C for



12 h in a PTFE autoclave. Then, CNTs/S, Super P, and polyvinylidene fluoride (PVDF) with weight ratio of 8:1:1 was mixed in N-methylpyrrolidone solution to prepare sulfur cathode slurry. Subsequently, the slurry was uniformly cast on the rough surface of aluminum foil and dried at 60 °C for 10 h, and the areal sulfur loading of active material was about 1 mg·cm<sup>-2</sup>. Finally, transition layer (Super P:PEO:LiTFSI = 5:3:2 by weight) with the thickness of about 20 μm was coated on the surface of the dried electrode to reduce the interfacial resistance.

### 2.3 Material characterization

Scanning electron microscope (SEM, MERLIN Compact) was used to observe the surface and cross-sectional morphology of the films. The stress and strain of the material were measured by a universal mechanical testing machine (CMT6103) at a rate of 10 mm·min<sup>-1</sup>. Thermogravimetry (TG, TGA2050) was used to test the thermal stability of the electrolyte membrane in the temperature range of 25–600 °C at the heating rate of 10 °C·min<sup>-1</sup> under N<sub>2</sub> flow. X-ray diffraction (XRD, Bruker D8, Germany) was used to analyze the structure and crystallinity of electrolytes.

### 2.4 Electrochemical test

All batteries were assembled in an argon-filled glove box with a standard 2032 coin cell configuration. The cyclic voltammetry (CV) and electrochemical impedance spectroscopy (EIS) measurements were performed on an electrochemical workstation (CHI660E, CH Instrument). The ionic conductivity ( $\sigma$ ) of electrolytes was analyzed by measuring alternating current (AC) impedance spectra of SS/SS (stainless steel) cells through electrochemical workstation (CHI660E, CH Instrument) in the frequency range of 0.1 Hz to 1 MHz with AC amplitude of 10 mV from 25 to 60 °C, and calculated according to the following Eq. (1):

$$\sigma = \frac{L}{R \cdot S} \quad (1)$$

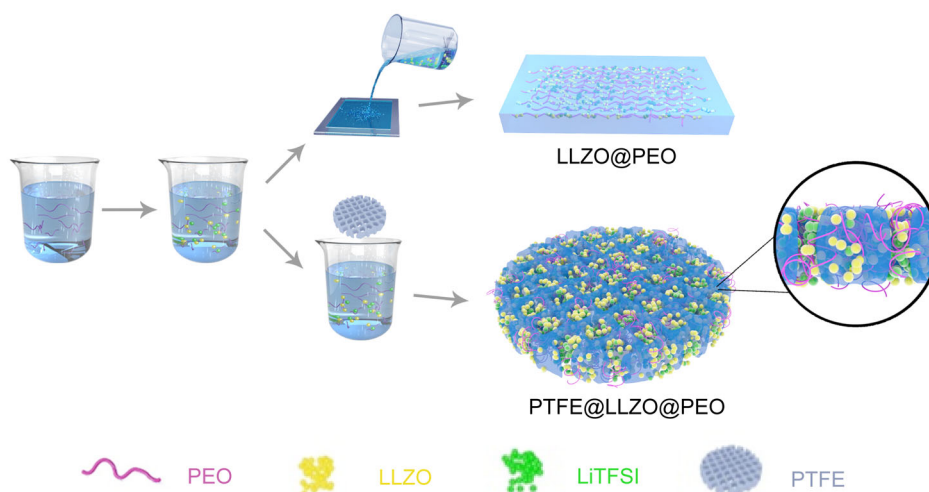
where  $L$  and  $R$  represent the thickness and bulk resistance of the electrolyte, respectively.  $S$  represents the contact area between electrolyte and stainless-steel electrode. In addition, the impedance of SS/electrolyte/Li at 30 °C was tested by the same method. The CV curves of S/electrolyte/Li were obtained in the voltage range of 1.7–3.3 V at 0.05 mV·s<sup>-1</sup>. The charge–discharge performance of S/electrolyte/Li battery between 1.7 and 2.8 V (Li<sup>+</sup>/Li) was tested by LAND CT2001 battery test system.

## 3 Results and discussion

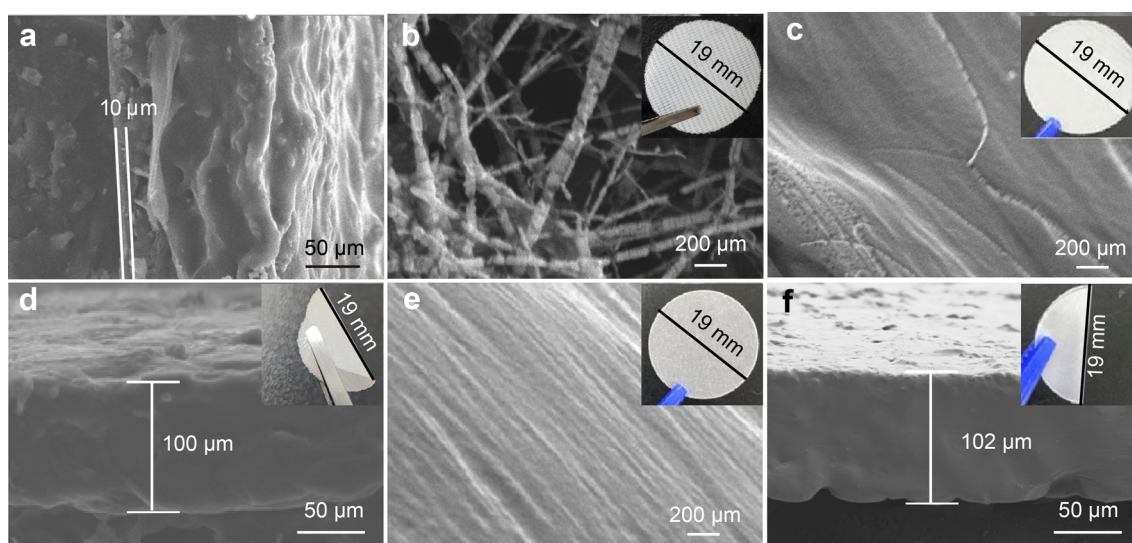
The preparation methods of LLZO@PEO solid electrolyte and PTFE@LLZO@PEO solid electrolyte are shown in Fig. 1. First, PEO, lithium salt, and LLZO particles were uniformly mixed in anhydrous acetonitrile to obtain LLZO@PEO slurry. Then, the uniformly mixed LLZO@PEO solution was poured into the PTFE mold, and the LLZO@PEO electrolyte membrane was obtained after drying. In addition, to obtain PTFE@LLZO@PEO solid electrolyte, PTFE porous membrane was immersed in LLZO@PEO solution and stirred for a period of time to ensure that the pores were fully filled with liquid. Subsequently, PTFE membrane completely infiltrated by LLZO@PEO solution was dried and rolled to obtain PTFE@LLZO@PEO solid electrolyte membrane.

Figure 2a shows the cross-sectional morphology of cathode bonded with electrolyte, and it can be seen that the cathode is closely contacted with the electrolyte via the interface buffer layer, and the thickness of the interface buffer layer is about 10 μm. The novel structural design ensures the close adhesion of the electrolyte layer and the electrode, which can greatly reduce the interfacial impedance caused by poor interface contact. Figure 2b is SEM and optical photographs of PTFE porous membrane. It clearly shows the porous structure of the three-dimensional skeleton formed by the interwoven connection of the skeleton, and the pore size is about 250 nm. After immersing the PTFE skeleton into the PEO-based solution, the PEO-based solution has completely filled into the pores of the PTFE skeleton, and no splitting or stratification is observed (Fig. 2c). The PTFE@LLZO@PEO electrolyte membrane with the thickness of 100 μm is uniformly distributed (Fig. 2d). The uniform PTFE network structure can provide the electrolyte membrane with excellent mechanical properties, and LLZO@PEO can endow the electrolyte membrane with smooth surface (Fig. 2e), which is conducive to reducing the impedance and improving the cycle life of the battery [55]. The thickness of LLZO@PEO electrolyte film is about 102 μm (Fig. 2f).

In order to further detect the phase composition and crystallinity of the electrolyte, PTFE@LLZO@PEO electrolyte membrane and LLZO@PEO electrolyte membrane were tested by XRD. PEO exhibits two characteristic diffraction peaks at  $2\theta = 19^\circ$  and  $23^\circ$ , while the intensity of PEO crystallization peak decreases significantly after the introduction of LLZO particles and PTFE skeleton (Fig. 3a). The increase of amorphous phase can be attributed to the physical interaction between PTFE, LLZO, and PEO, which hinders the orderly arrangement of PEO segments. The mechanical properties of PTFE membrane and PTFE@LLZO@PEO electrolyte membrane were evaluated by tensile strength test (Fig. 3b). The maximum tensile



**Fig. 1** Preparation process of LLZO@PEO and PTFE@LLZO@PEO solid electrolyte membrane



**Fig. 2** **a** SEM image of cross section of positive electrode bonded with electrolyte; **b** surface morphology of PTFE porous membrane, (inset being photo of PTFE porous membrane); **c** surface morphology of PTFE@LLZO@PEO electrolyte film (inset being photo of PTFE@LLZO@PEO electrolyte); **d** cross-sectional morphology of PTFE@LLZO@PEO electrolyte (inset showing a curved PTFE@LLZO@PEO electrolyte); **e** surface morphology of LLZO@PEO electrolyte film (inset being photo of LLZO@PEO electrolyte); **f** cross-sectional morphology of LLZO@PEO electrolyte (inset showing a curved LLZO@PEO electrolyte)

strength and strain of PTFE membrane are 3.7 MPa and 35.33%, respectively. After filling with LLZO@PEO, the maximum tensile strength and strain increase to 4.82 MPa and 73.33%, respectively. The toughness improvement of PTFE@LLZO@PEO electrolyte membrane compared to PTFE membrane is attributed to the synergistic effect of LLZO@PEO and PTFE skeleton. The thermal stability of PTFE@LLZO@PEO electrolyte membrane was evaluated by TG. PTFE@LLZO@PEO electrolyte has no obvious weight loss before 375 °C, indicating that

PTFE@LLZO@PEO electrolyte has good thermal stability. The decomposition temperature of PTFE@LLZO@PEO electrolyte is about 375 °C, slightly higher than that of LLZO@PEO electrolyte (365 °C), which is attributed to the shielding effect provided by highly thermally stable LLZO and PTFE skeleton (Fig. 3c) [56]. Electrochemical stability is also an important index to evaluate the electrochemical potential and safety of solid electrolyte [53]. Figure 3d shows LSV curves of PTFE@LLZO@PEO electrolyte and PEO@LLZO electrolyte, in which

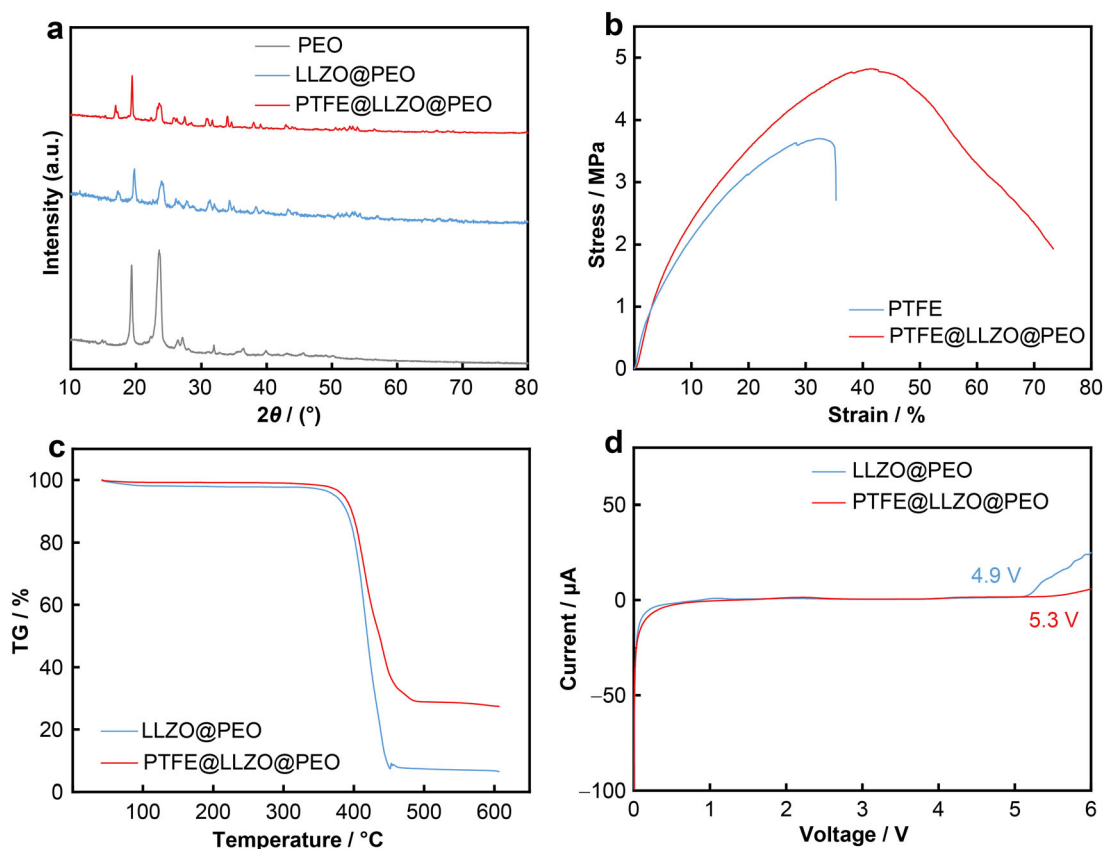


**Fig. 3** **a** XRD patterns of PTFE@LLZO@PEO electrolyte, PEO@LLZO electrolyte, and PEO; **b** stress–strain curves of PTFE@LLZO@PEO electrolyte and LLZO@PEO electrolyte; **c** TG curves of PTFE@LLZO@PEO electrolyte and PEO@LLZO electrolyte; **d** linear voltammetry curves of PTFE@LLZO@PEO electrolyte and PEO@LLZO electrolyte

PEO@LLZO electrolyte shows 4.9 V oxidation voltage, and the oxidation voltage of PTFE@LLZO@PEO electrolyte further increases to 5.3 V. The electrochemical windows of these two electrolytes can fully meet the needs of lithium–sulfur batteries. Moreover, the electrolyte prepared can also be applied in high-voltage lithium battery system, e.g., NCM or lithium-rich cathode materials. It has been reported that electrolyte systems with lower HOMO (the highest occupied molecular orbital) levels have higher oxidation resistance [57], and PTFE has a lower HOMO energy level, that is, it has better high-voltage tolerance. In addition, the F atom in PTFE will form hydrogen bonds with the H atom in PEO, which improves the oxidation resistance of PEO component, and then improves the overall oxidation resistance of the electrolyte.

Figure 4a–c shows the effect of temperature on the ionic conductivity of PTFE@LLZO@PEO and LLZO@PEO solid electrolytes. With the increase of temperature, the impedance of electrolyte gradually decreases, which can be ascribed to that the vibration and swing of polymer chains are strengthened and the mobility of transfer ions is enhanced at high temperatures. The ionic conductivity of

PTFE@LLZO@PEO solid electrolyte was  $3.48 \times 10^{-5} \text{ S}\cdot\text{cm}^{-1}$  at room temperature,  $5.03 \times 10^{-5} \text{ S}\cdot\text{cm}^{-1}$  at  $30^{\circ}\text{C}$ , and  $2.54 \times 10^{-4} \text{ S}\cdot\text{cm}^{-1}$  at  $60^{\circ}\text{C}$ , which is higher than that of LLZO@PEO electrolyte at the same temperature. It can be attributed to the fact that the PTFE three-dimensional framework can be seen as a  $\text{Li}^{+}$  diffusion channel to assist ion diffusion, thus facilitating the transmission of  $\text{Li}^{+}$  in electrolyte. The introduction of LLZO can inhibit the crystallization of PEO, thereby improving the ionic conductivity of PEO matrix. Furthermore, due to the interaction of acidic or alkaline groups on the surface of LLZO with polymer matrix and lithium salt, the dissociation of lithium salt can be promoted, thereby forming a channel conducive to lithium-ion diffusion on the surface of LLZO ceramic particles [58]. Lithium symmetric batteries can be used to characterize the interfacial stability between electrolyte and lithium metal and test the ability of electrolyte to inhibit the growth of lithium dendrites. Figure 4d shows the cycle performance of the Li|PTFE@LLZO@PEO|Li symmetric battery at  $30^{\circ}\text{C}$  and the current density of  $0.1 \text{ mA}\cdot\text{cm}^{-2}$ . The voltage gap of the battery with LLZO@PEO solid electrolyte suddenly increased and

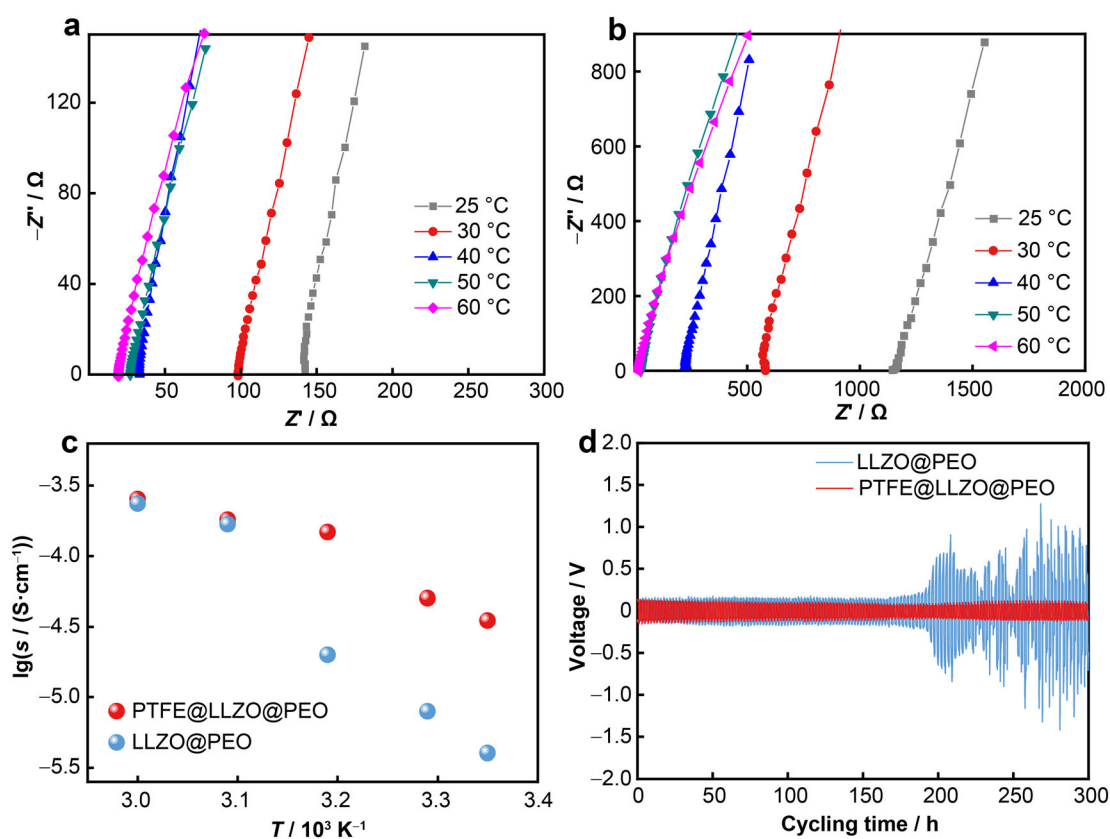


**Fig. 4** **a** Impedance spectra of PTFE@LLZO@PEO solid electrolyte at different temperatures; **b** impedance spectra of LLZO@PEO solid electrolyte at different temperatures; **c** ionic conductivity of PTFE@LLZO@PEO and LLZO@PEO electrolytes at different temperatures; **d** cycling performance of Li|PTFE@LLZO@PEO|Li and Li|LLZO@PEO|Li batteries at  $0.1 \text{ mA}\cdot\text{cm}^{-2}$

fluctuated after 190 h of stable cycle, which may be related to the growth of lithium dendrites in electrolyte. While the battery with PTFE@LLZO@PEO solid electrolyte remained stable after 300 h of cycling and maintained a low overpotential (about 0.15 V). This shows that the introduction of 3D-PTFE skeleton in LLZO@PEO electrolyte can promote the uniform deposition of  $\text{Li}^+$ .

In order to study the redox reaction and electrochemical stability of PTFE@LLZO@PEO solid electrolyte in lithium–sulfur battery, the CV curves of Li|PTFE@LLZO@PEO|S battery and Li|LLZO@PEO|S battery were performed at a scanning rate of  $0.05 \text{ mV}\cdot\text{s}^{-1}$ . As shown in Fig. 5a, b, CV curves of Li–S batteries containing LLZO@PEO solid electrolyte have two obvious reduction peaks at 2.0 and 2.3 V, corresponding to the long-chain polysulfides ( $2.3 \text{ V}/\text{Li}_2\text{S}_x$ ,  $x > 4$ ) and short-chain polysulfides ( $2.0 \text{ V}/\text{Li}_2\text{S}_2$  and  $\text{Li}_2\text{S}$ ), respectively. However, the CV curve of the battery containing PTFE@LLZO@PEO solid electrolyte shows an obvious reduction peak near 2.3 V, and the peak near 2.0 V coincides with the curve completely, which indicates that the long-chain polysulfides and short-chain polysulfides in the two stages are combined during discharge, indicating that PEO@LLZTO

electrolyte cannot completely inhibit the diffusion of polysulfides. However, benefiting from the dense three-dimensional skeleton structure of PTFE, PTFE@LLZO@PEO electrolyte can better hinder and adsorb polysulfides to reduce the shuttle effect of polysulfides.

The cycle stability and rate performance of the solid-state lithium sulfur battery with PTFE@LLZO@PEO electrolyte and LLZO@PEO electrolyte was evaluated at  $30 \text{ }^\circ\text{C}$  and 1.7–2.8 V. Figure 5c shows the discharge/charge curve of Li|PTFE@LLZO@PEO|S battery and Li|LLZO@PEO|S battery at 0.10C. The initial discharge capacity of Li|PTFE@LLZO@PEO|S battery is  $655 \text{ mAh}\cdot\text{g}^{-1}$ , and the discharge capacity remains at  $568 \text{ mAh}\cdot\text{g}^{-1}$  after 100 cycles, with a capacity retention of 86%. In contrast, the initial discharge capacity of Li|LLZO@PEO|S battery is  $663 \text{ mAh}\cdot\text{g}^{-1}$ , but the capacity retention is only 64% after 100 cycles. This can be attributed to the introduction of PTFE skeleton that is more conducive to inhibiting the growth of lithium dendrites and weakening the shuttle of polysulfides. In addition, the performance at different rates is shown in Fig. 5d. First, the battery was cycled 10 times at 0.05C, and then the rate performance of the battery was tested at 0.10C, 0.50C,

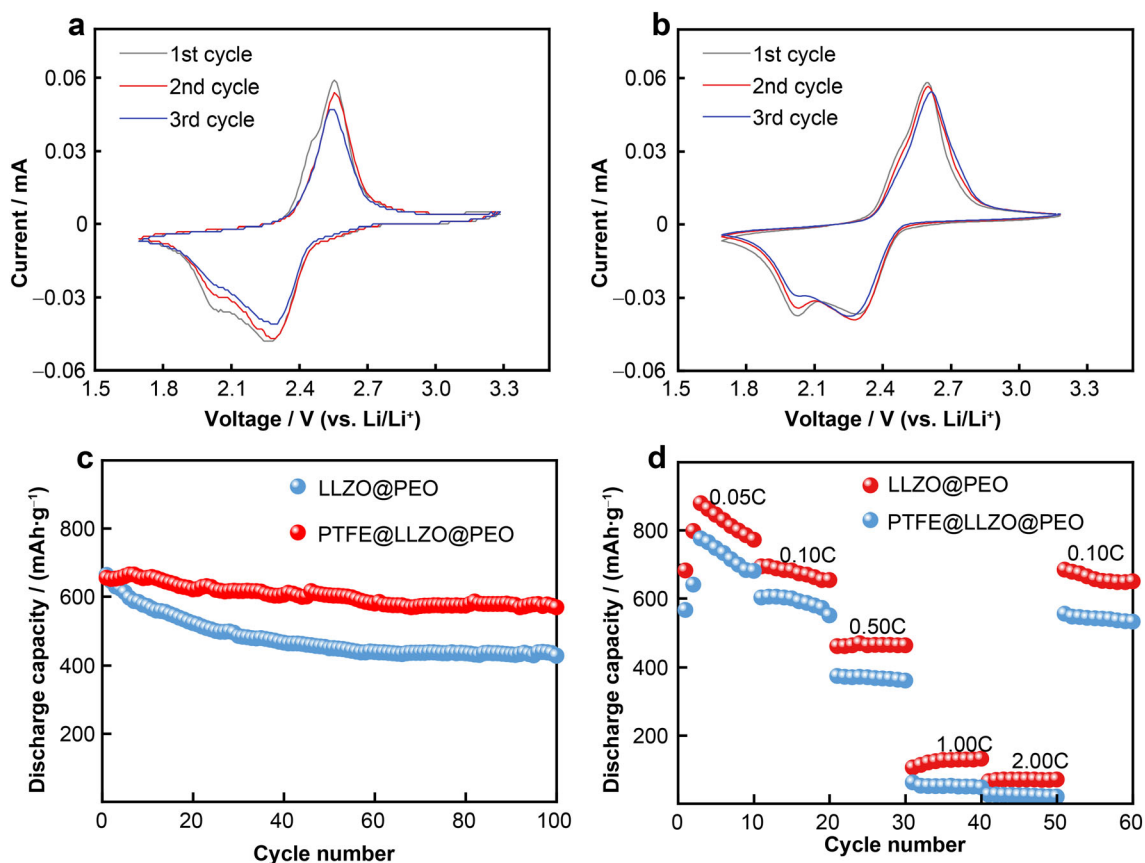


**Fig. 5** **a** Cyclic voltammogram of Li|PTFE@LLZO@PEO|S battery; **b** cyclic voltammogram of Li|LLZO@PEO|S battery; **c** cycling performance of Li|PTFE@LLZO@PEO|S and Li|LLZO@PEO|S battery; **d** rate performance of Li|PTFE@LLZO@PEO|S and Li|LLZO@PEO|S battery

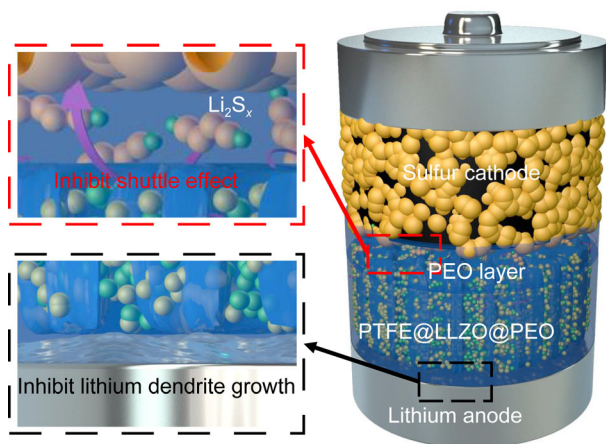


**Fig. 6** Schematic illustration showing multi-functional effect of PTFE@LLZO@PEO electrolyte in lithium–sulfur battery

1.00C, 2.00C and 0.10C (10 cycles per rate). At the current densities of 0.10C, 0.50C, 1.00C and 2.00C, the discharge-specific capacities of Li|PTFE@LLZO@PEO|S cells were 694.6, 460.2, 105.8 and 69.7 mAh·g<sup>-1</sup>, while those of Li|LLZO@PEO|S cells were only 603.5, 374.3, 61.4 and 26.4 mAh·g<sup>-1</sup>, respectively. Obviously, the battery with PTFE@LLZO@PEO has better rate performance.

Figure 6 shows the multi-functional effect of PTFE@LLZO@PEO electrolyte in lithium–sulfur battery. Firstly, PTFE@LLZO@PEO electrolyte can effectively inhibit the shuttle effect of lithium polysulfide and reduce the side reactions of lithium polysulfide and lithium metal. The structural design of PEO layer is conducive to reducing the interfacial impedance between the electrolyte and the cathode, and ensuring the close adhesion between the electrolyte layer and the electrode. Secondly, PTFE@LLZO@PEO electrolyte can promote the uniform deposition of Li<sup>+</sup>, thereby inhibiting the growth of lithium dendrites. In addition, PTFE has excellent non-flammability and thermal stability, which further enhances the safety

performance of lithium–sulfur batteries using PTFE@LLZO@PEO electrolyte.

#### 4 Conclusion

In summary, the PTFE membrane was introduced into the PEO@LLZO-based composite electrolyte as a supporting structure to prepare a new PTFE composite electrolyte (PTFE@LLZO@PEO), which was used for all-solid-state lithium–sulfur batteries. The introduction of PTFE membrane greatly improved the thermal stability and mechanical properties of the electrolyte membrane. The electrolyte membrane showed good ionic conductivity, which was  $3.8 \times 10^{-5} \text{ S}\cdot\text{cm}^{-1}$  at room temperature and  $2.54 \times 10^{-4} \text{ S}\cdot\text{cm}^{-1}$  at 60 °C. The Li|PTFE@LLZO@PEO|S battery showed an initial discharge capacity of 680 mAh·g<sup>-1</sup> at 0.10C and a capacity retention of 86% after 100 cycles. Moreover, the electrolyte used in all-solid-state lithium–sulfur battery has good cycle stability and rate performance, and can significantly inhibit the shuttle effect of lithium polysulfide. In addition, this work provides guidance for the rational design of composite solid-state electrolytes and high-performance all-solid-state lithium–sulfur batteries.

**Acknowledgements** This work was financially supported by the Talents Project of Beijing Municipal Committee Organization Department (No. 2018000021223ZK21), the Fundamental Research Funds for the Central Universities (No. 2021JCCXJD01), Key R&D and Transformation Projects in Qinghai Province (No. 2021-HZ-808) and Hebei Province (No. 21314401D), Open Funds of Chongqing Key Laboratory of Green Aviation Energy and Power (No. GATRI2021F01003B).

#### Declarations

**Conflict of interests** The authors declare that they have no conflict of interest.

#### References

- [1] Chai J, Liu Z, Zhang J, Sun J, Tian Z, Ji Y, Tang K, Zhou X, Cui G. A superior polymer electrolyte with rigid cyclic carbonate backbone for rechargeable lithium ion batteries. *ACS Appl Mater Interfaces*. 2017;9(21):17897.
- [2] Wu F, Chu F, Ferrero GA, Sevilla M, Fuertes AB, Borodin O, Yu Y, Yushin G. Boosting high-performance in lithium–sulfur batteries via dilute electrolyte. *Nano Lett*. 2020;20(7):5391.
- [3] Wu PF, Shi BY, Tu HB, Guo CQ, Liu AH, Yan G, Yu UZJ. Pomegranate-type Si/C anode with SiC taped, well-dispersed tiny Si particles for lithium-ion batteries. *J Adv Ceram*. 2021;10(5):1129.
- [4] Gao ZG, Zhang SJ, Huang ZG, Liu Q, Wang WW, Li JT. Protection of Li metal anode by surface-coating of PVDF thin film to enhance the cycling performance of Li batteries. *Chin Chem Lett*. 2019;30(2):525.
- [5] Wu X, Liang X, Zhang X, Lan L, Li S, Gai Q. Structural evolution of plasma sprayed amorphous Li<sub>4</sub>Ti<sub>5</sub>O<sub>12</sub> electrode and ceramic/polymer composite electrolyte during electrochemical cycle of quasi-solid-state lithium battery. *J Adv Ceram*. 2021;10(2):347.
- [6] Ma Y. Computer simulation of cathode materials for lithium ion and lithium batteries: a review. *Energy Environ Mater*. 2018;1(3):148.
- [7] Zhao M, Li BQ, Zhang XQ, Huang JQ, Zhang Q. A perspective toward practical lithium–sulfur batteries. *ACS Cent Sci*. 2020;6(7):1095.
- [8] Wang WP, Zhang J, Chou J, Yin YX, You Y, Xin S, Guo YG. Solidifying cathode–electrolyte interface for lithium–sulfur batteries. *Adv Energy Mater*. 2020;11(2):2000791.
- [9] Ye H, Li M, Liu T, Li Y, Lu J. Activating Li<sub>2</sub>S as the lithium-containing cathode in lithium–sulfur batteries. *ACS Energy Lett*. 2020;5(7):2234.
- [10] Gonzalez Puente PM, Song SB, Cao SY, Rannalter LZ, Pan ZW, Xiang X, Shen Q, Chen F. Garnet-type solid electrolyte: advances of ionic transport performance and its application in all-solid-state batteries. *J Adv Ceram*. 2021;10(5):933.
- [11] Xie YL, Kong JR, Pan D, Liu XN, Zhou T. Preparation and performance study of La<sub>0.75</sub>Sr<sub>0.25</sub>Cr<sub>0.5</sub>Mn<sub>0.5</sub>O<sub>3-δ</sub>-Ce<sub>0.8</sub>Gd<sub>0.2</sub>O<sub>2-δ</sub> gradient composite cathode for solid oxide electrolysis cell. *Chin J Rare Met*. 2021;45(11):1343.
- [12] Wang Y, Ji H, Zhang X, Shi J, Li X, Jiang X, Qu X. Cyclopropenium cationic-based covalent organic polymer-enhanced poly(ethylene oxide) composite polymer electrolyte for all-solid-state Li-S battery. *ACS Appl Mater Interfaces*. 2021;13(14):16469.
- [13] Tesio AY, Gomez-Camer JL, Morales J, Caballero A. Simple and sustainable preparation of nonactivated porous carbon from brewing waste for high-performance lithium–sulfur batteries. *Chemsuschem*. 2020;13(13):3439.
- [14] Qiu Y, Yin XJ, Wang MX, Li M, Sun X, Jiang B, Zhou H, Tang DY, Zhang Y, Fan LS, Zhang NQ. Constructed conductive CoSe<sub>2</sub> nanoarrays as efficient electrocatalyst for high-performance Li–S battery. *Rare Met*. 2021;40(11):3147.
- [15] Yang X, Li XT, Zhao CF, Fu ZH, Zhang QS, Hu C. Promoted deposition of three-dimensional Li<sub>2</sub>S on catalytic Co phthalocyanine nanorods for stable high-loading lithium–sulfur batteries. *ACS Appl Mater Interfaces*. 2020;12(29):32752.
- [16] Pan Y, Cheng X, Gao M, Fu Y, Feng J, Ahmed H, Gong L, Zhang H, Battaglia VS. Dual-functional multichannel carbon framework embedded with CoS<sub>2</sub> nanoparticles: promoting the phase transformation for high-loading Li-S batteries. *ACS Appl Mater Interfaces*. 2020;12(29):32726.
- [17] Yang M, Shi D, Sun X, Li Y, Liang Z, Zhang L, Shao Y, Wu Y, Hao X. Shuttle confinement of lithium polysulfides in borocarbonitride nanotubes with enhanced performance for lithium–sulfur batteries. *J Mater Chem A*. 2020;8(1):296.
- [18] Yang Q, Deng N, Chen J, Cheng B, Kang W. The recent research progress and prospect of gel polymer electrolytes in lithium–sulfur batteries. *Chem Eng J*. 2021;413:127427.
- [19] Shao D, Yang L, Luo K, Chen M, Zeng P, Liu H, Liu L, Chang B, Luo Z, Wang X. Preparation and performances of the modified gel composite electrolyte for application of quasi-solid-state lithium sulfur battery. *Chem Eng J*. 2020;389:124300.
- [20] Xia Y, Liang YF, Xie D, Wang XL, Zhang SZ, Xia XH, Gu CD, Tu JP. A poly(vinylidene fluoride-hexafluoropropylene) based three-dimensional network gel polymer electrolyte for solid-state lithium–sulfur batteries. *Chem Eng J*. 2019;358:1047.
- [21] Cao D, Sun X, Li Q, Natan A, Xiang P, Zhu H. Lithium dendrite in all-solid-state batteries: growth mechanisms, suppression strategies, and characterizations. *Matter*. 2020;3(1):57.





- [22] Li Y, Guo XT, Zhang ST, Pang H. Promoting performance of lithium–sulfur battery via in situ sulfur reduced graphite oxide coating. *Rare Met.* 2020;40(2):417.
- [23] Yang Y, Chen C, Hu J, Deng Y, Zhang Y, Yang D. High performance lithium–sulfur batteries by facilely coating a conductive carbon nanotube or graphene layer. *Chin Chem Lett.* 2018; 29(12):1777.
- [24] Chen WJ, Zhao CX, Li BQ, Jin Q, Zhang XQ, Yuan TQ, Zhang X, Jin Z, Kaskel S, Zhang Q. A mixed ether electrolyte for lithium metal anode protection in working lithium–sulfur batteries. *Energy Environ Mater.* 2020;3(2):160.
- [25] Andreas Arie A, Lenora S, Kristianto H, Frida Susanti R, Kee LJ. Potato peel based carbon-sulfur composite as cathode materials for lithium sulfur battery. *J Nanosci Nanotechnol.* 2021;21(12):6243.
- [26] Zhu L, Hu RW, Xiang YH, Yang XX, Chen Z, Xiong LZ, Wu XW, He ZQ, Lei WX. Enhanced performance of Li-S battery by constructing inner conductive network and outer adsorption layer sulfur-carbon composite. *Int J Energy Res.* 2021;45(4): 6002.
- [27] Liu KF, Zhao HB, Ye DX, Zhang JJ. Recent progress in organic polymers-composited sulfur materials as cathodes for lithium–sulfur battery. *Chem Eng J.* 2021;417:129309.
- [28] Li XC, Zhang Y, Wang ST, Liu Y, Ding Y, He GH, Jiang XB, Xiao W, Yu GH. Scalable high-areal-capacity Li-S batteries enabled by sandwich-structured hierarchically porous membranes with intrinsic polysulfide adsorption. *Nano Lett.* 2020; 20(9):6922.
- [29] Man LM, Yang Y, Wang H, Wang YY, An YN, Bao JL, Wang CY, Yang ZH. In situ-cross-linked supramolecular eco-binders for improved capacity and stability of lithium–sulfur batteries. *ACS Appl Energy Mater.* 2021;4(4):3803.
- [30] Chen H, Wu ZZ, Su Z, Hencz L, Chen S, Yan C, Zhang SQ. A hydrophilic poly(methyl vinyl ether-alt-maleic acid) polymer as a green, universal, and dual-functional binder for high-performance silicon anode and sulfur cathode. *J Energy Chem.* 2021; 62:127.
- [31] Eshetu GG, Judez X, Li C, Bondarchuk O, Rodriguez-Martinez LM, Zhang H, Armand M. Lithium Azide as an electrolyte additive for all-solid-state lithium–sulfur batteries. *Angew Chem Int Ed Engl.* 2017;56(48):15368.
- [32] Hong S, Wang Y, Kim N, Lee SB. Polymer-based electrolytes for all-solid-state lithium–sulfur batteries: from fundamental research to performance improvement. *J Mater Sci.* 2021; 56(14):8358.
- [33] Xu B, Li X, Yang C, Li Y, Grundish NS, Chien PH, Dong K, Manke I, Fang R, Wu N, Xu H, Dolocan A, Goodenough JB. Interfacial chemistry enables stable cycling of all-solid-state Li metal batteries at high current densities. *J Am Chem Soc.* 2021; 143(17):6542.
- [34] Ding WQ, Lv F, Xu N, Wu MT, Liu J, Gao XP. Polyethylene oxide-based solid-state composite polymer electrolytes for rechargeable lithium batteries. *ACS Appl Energy Mater.* 2021; 4(5):4581.
- [35] Banerjee A, Wang XF, Fang CC, Wu EA, Meng YS. Interfaces and interphases in all-solid-state batteries with inorganic solid electrolytes. *Chem Rev.* 2020;120(14):6878.
- [36] Yan CL. Realizing high performance of solid-state lithium metal batteries by flexible ceramic/polymer hybrid solid electrolyte. *Rare Met.* 2020;39(5):458.
- [37] Jin Y, Zong X, Zhang X, Liu C, Li D, Jia Z, Li G, Zhou X, Wei J, Xiong Y. Interface regulation enabling three-dimensional  $\text{Li}_{1.3}\text{Al}_{0.3}\text{Ti}_{1.7}(\text{PO}_4)_3$ -reinforced composite solid electrolyte for high-performance lithium batteries. *J Power Sources.* 2021;501: 230027.
- [38] Wang S, Sun Q, Peng W, Ma Y, Zhou Y, Song D, Zhang H, Shi X, Li C, Zhang L. Ameliorating the interfacial issues of all-solid-state lithium metal batteries by constructing polymer/inorganic composite electrolyte. *J Energy Chem.* 2021;58:85.
- [39] Chen H, Zhou CJ, Dong XR, Yan M, Liang JY, Xin S, Wu XW, Guo YG, Zeng XX. Revealing the superiority of fast ion conductor in composite electrolyte for dendrite-free lithium-metal batteries. *ACS Appl Mater Interfaces.* 2021;13(19):22978.
- [40] Zhu X, Wang K, Xu Y, Zhang G, Li S, Li C, Zhang X, Sun X, Ge X, Ma Y. Strategies to boost ionic conductivity and interface compatibility of inorganic-organic solid composite electrolytes. *Energy Storage Mater.* 2021;36:291.
- [41] Yu Q, Jiang K, Yu C, Chen X, Zhang C, Yao Y, Jiang B, Long H. Recent progress of composite solid polymer electrolytes for all-solid-state lithium metal batteries. *Chin Chem Lett.* 2021; 32(9):2659.
- [42] Li X, Wang D, Wang H, Yan H, Gong Z, Yang Y. Poly(ethylene oxide)- $\text{Li}_{10}\text{SnP}_2\text{S}_{12}$  composite polymer electrolyte enables high-performance all-solid-state lithium sulfur battery. *ACS Appl Mater Interfaces.* 2019;11(25):22745.
- [43] Fang R, Xu B, Grundish NS, Xia Y, Li Y, Lu C, Liu Y, Wu N, Goodenough JB.  $\text{Li}_2\text{S}_6$ -integrated PEO-based polymer electrolytes for all-solid-state lithium-metal batteries. *Angew Chem Int Ed Engl.* 2021;60(32):17701.
- [44] Lee F, Tsai MC, Lin MH, Ni'mah YL, Hy S, Kuo CY, Cheng JH, Rick J, Su WN, Hwang BJ. Capacity retention of lithium sulfur batteries enhanced with nano-sized  $\text{TiO}_2$ -embedded polyethylene oxide. *J Mater Chem A.* 2017;5(14):6708.
- [45] Kou W, Wang J, Li W, Lv R, Wang J. Asymmetry-structure electrolyte with rapid  $\text{Li}^+$  transfer pathway towards high-performance all-solid-state lithium–sulfur battery. *J Membr Sci.* 2021;634:119432.
- [46] Tao X, Liu Y, Liu W, Zhou G, Yi C. Solid-state lithium–sulfur batteries operated at 37 °C with composites of nanostructured  $\text{Li}_7\text{La}_3\text{Zr}_2\text{O}_{12}$ /carbon foam and polymer. *Nano Lett.* 2017;17(5): 2967.
- [47] Wang C, Yang Y, Liu X, Zhong H, Xu H, Xu Z, Shao H, Ding F. Suppression of lithium dendrite formation by using LAGP-PEO ( $\text{LiTFSI}$ ) composite solid electrolyte and lithium metal anode modified by PEO ( $\text{LiTFSI}$ ) in all-solid-state lithium batteries. *Acs Appl Mater Interfaces.* 2017;9(15):13694.
- [48] Fang R, Xu H, Xu B, Li X, Li Y, Goodenough JB. Reaction mechanism optimization of solid-state Li–S batteries with a PEO-based electrolyte. *Adv Funct Mater.* 2020;31(2):2001812.
- [49] Song S, Wu Y, Tang W, Deng F, Yao J, Liu Z, Hu R, Alamusi ZW, Lu L, Hu N. Composite solid polymer electrolyte with garnet nanosheets in poly(ethylene oxide). *ACS Sustain Chem Eng.* 2019;7(7):7163.
- [50] Li Y, Han JT, Wang CA, Xie H, Goodenough JB. Optimizing  $\text{Li}^+$  conductivity in a garnet framework. *J Mater Chem.* 2012; 22(30):15357.
- [51] Ji Y, Yang K, Liu M, Chen S, Liu X, Yang B, Wang Z, Huang W, Song Z, Xue S, Fu Y, Yang L, Miller TS, Pan F. PIM-1 as a multifunctional framework to enable high-performance solid-state lithium–sulfur batteries. *Adv Funct Mater.* 2021;31(47): 2104830.
- [52] Jiang T, He P, Wang G, Shen Y, Fan LZ. Solvent-free synthesis of thin, flexible, nonflammable garnet-based composite solid electrolyte for all-solid-state lithium batteries. *Adv Energy Mater.* 2020;10(12):1903376.
- [53] Hippauf F, Schumm B, Doerfler S, Althues H, Fujiki S, Shiratsuchi T, Tsujimura T, Aihara Y, Kaskel S. Overcoming binder limitations of sheet-type solid-state cathodes using a solvent-free dry-film approach. *Energy Storage Mater.* 2019;21: 390.

- [54] Delluva AA, Kulberg-Savercool J, Holewinski A. Decomposition of trace  $\text{Li}_2\text{CO}_3$  during charging leads to cathode interface degradation with the solid electrolyte LLZO of trace  $\text{Li}_2\text{CO}_3$  during charging leads to cathode interface degradation with the solid electrolyte LLZO. *Adv Func Mater.* 2021;31(34):2103716.
- [55] Li W, Wang Q, Jin J, Li Y, Wu M, Wen Z. Constructing dual interfacial modification by synergetic electronic and ionic conductors: toward high-performance LAGP-based Li-S batteries. *Energy Storage Mater.* 2019;23:299.
- [56] Nagajothi AJ, Kannan R, Rajashabala S. Studies on electrochemical properties of poly (ethylene oxide)-based gel polymer electrolytes with the effect of chitosan for lithium–sulfur batteries. *Polym Bull.* 2017;74(12):4887.
- [57] Zhou Q, Ma J, Dong S, Li X, Cui G. Intermolecular chemistry in solid polymer electrolytes for high-energy-density lithium batteries. *Adv Mater.* 2019;31(50):1902029.
- [58] Bae J, Li Y, Zhang J, Zhou X, Zhao F, Shi Y, Goodenough JB, Yu G. A 3D nanostructured hydrogel-framework-derived high-performance composite polymer lithium-ion electrolyte. *Angew Chem Int Ed Engl.* 2018;57(8):2096.